BEYOND GROUND CONTROL POINTS: COST-EFFECTIVE 3D BUILDING RECONSTRUCTION THROUGH GNSS-INTEGRATED PHOTOGRAMMETRY

E. Oniga [a], B. Boroianu [b], L. Morelli [c,d], F. Remondino [c], M. Macovei [a]

[a] Department of Terrestrial Measurements and Cadastre, Technical University „Gheorghe Asachi" of Iasi, D. Mangeron Street, Iasi, Romania – <valeria-ersilia.oniga><mihaela.macovei>@academic.tuiasi.ro

[b] Geocad Profesional SRL (Smart Imaging and Mapping Services-SIMS); office@sims.ro

[c] 3D Optical Metrology (3DOM) unit, Bruno Kessler Foundation (FBK), Trento, Italy - (lmorelli)(remondino)@fbk.eu

[d] Dept. of Civil, Environmental and Mechanical Engineering (DICAM), University of Trento, Italy

Commission II

KEY WORDS: RTK/PPK integrated system, GNSS-assisted photogrammetry, direct georeferencing, GCP, 3D Building Modeling

ABSTRACT:
The process of 3D building modeling serves a multitude of practical and strategic purposes across diverse industries. Building a 3D model involves employing a range of techniques and technologies. Among these, the most used methods include 3D laser scanning and photogrammetry, whether applied at close-range or through the use of Unmanned Aerial Systems (UAS). In photogrammetry, ground control points (GCPs) are generally needed to scale and georeference the digital reconstruction process, but it is a time-consuming practice or sometimes impractical or dangerous. This paper aims to evaluate the efficiency of two integrated devices to perform photogrammetric 3D reconstruction without GCPs. They are both composed by a Sony ZV1 camera coupled with two different RTK/PPK GNSS system: the Emlid Reach RS2 GNSS receiver and the Emlid Reach M2 module with a multi-band GNSS helical antenna. Different sets of images were acquired with the two proposed devices for the lever-arm estimation and to perform the 3D surveying of the Galata monastery historical monument. The accuracy of the process and derived dense point clouds is assessed by comparing them with GCPs and a reference point cloud derived by fusing an UAS and a high-resolution mobile laser scanning point cloud. The ultimate goal is to obtain a 3D building model without the use of GCPs in the process of bundle block adjustment with centimeter accuracy.

1. INTRODUCTION

Building 3D modelling serves various practical and strategic purposes across several industries due to its capacity to enhance communication, decision-making, and efficiency across various stages of a building's lifecycle - from design and construction to management and preservation. Various applications such as urban planning and development, architectural design and visualization construction and engineering, real estate marketing, heritage preservation and documentation, environmental impact assessment, virtual and augmented reality experiences, heavily depend on the utilization of 3D buildings models (Wang, 2013; Xue et al., 2021; Ying et al., 2023).

The process of creating a building 3D model encompasses diverse techniques and technologies, with the most prevalent being 3D laser scanning and photogrammetry, whether conducted at close-range or with airborne platforms, including Unmanned Aerial Systems (UAS). The utilization of UASs equipped with Global Navigation Satellite System (GNSS) real-time kinematic (RTK) and post-processed kinematic (PPK) technologies can achieve centimeter accuracy for photogrammetric projects without the need for ground control points (GCPs), as shown in different studies (Przybilla et al., 2020; Zeybek, 2021; Nesbit et al., 2022; Oniga et al., 2023; Teppati et al., 2023; Zeybek et al., 2023). Equivalent solutions are also possible for terrestrial photogrammetry (Forlani et al., 2014; Jaud et al., 2020; Morelli et al., 2022; Eker 2023; Previtali et al., 2023; Teppati Losè et al., 2023). Compared with UAS photogrammetry for 3D building modelling, terrestrial photogrammetry has some advantages. Typically, the camera is close to the subject when acquiring images, resulting in higher ground sampling resolution. In addition, terrestrial photogrammetry does not face the same regulatory constraints as UAS operations, a significant advantage in areas where flying drones is restricted or requires special permits. Moreover, it is not as dependent on favourable weather conditions as UAS photogrammetry.

The private sector has released GNSS RTK rovers with Visual Positioning to the market. These devices can map hundreds of points from images acquired with a tilted or levelled pole, either in the field or in the office. This solution proves to be more robust and accurate in situations where GNSS signals might be obstructed or unreliable. Other commercial solutions integrate a camera with RTK/PPK GNSS antenna(s) for close-range photogrammetry applications, claiming centimeter accuracy.

While the idea of fusing photogrammetry with GNSS or GNSS/INS information has been around for 20 to 40 years, its widespread adoption for terrestrial applications has been limited by the high cost of these devices. So, over the years, researchers have tested various GNSS/INS devices integrated with a digital camera to achieve low-cost and time-effective methods for creating georeferenced results and accurate 3D reconstructions without the use of GCPs.

Nocerino et al. (2012) integrated a Nikon D3X with an u-blox GNSS receiver to achieve precise re-photographing results. Forlani et al. (2014) tested a device which included a digital camera and a GNSS receiver, with the antenna and the camera tied together on a geodetic pole, obtaining an absolute accuracy of 3-7 cm for several tests in an urban area. Morelli et al. (2022) proposed and tested a low-cost integrated system using an action cam and a low-cost GNSS antenna mounted on a geodetic pole for terrestrial GNSS-aided photogrammetry without GCPs. The RMSEs calculated for 12 check points are 1.3 cm in planimetry and 2.7 cm in altimetry, for the static approach and 1.3 cm and 2.2 cm for the horizontal and vertical accuracy respectively, in the case of kinematic approach. Jaud et al. (2020) tested a RTK system that integrates a GNSS antenna and a digital camera with the help of a wooden frame for coastal cliff monitoring, obtaining a standard deviation of 4.7 cm for the Nikon D800 Reflex camera and 3.8 cm, respectively, for the Huawei Y5 Smartphone camera, without using GCPs.

1.1 Aim of the work

The primary objective of this research is to propose and validate a comprehensive procedure that minimizes survey expenses and time requirements. The ultimate goal is to obtain a 3D building model without the use of GCPs within the photogrammetric processing.
Therefore, the aim of the paper is to test two different systems for GNSS-aided close-range photogrammetry (Table 1, Figure 1). Both systems are based on the Sony ZV1 digital camera (13.2 x 8.8 mm sensor, image resolution of 5472 x 3648 pixels, pixel size of 2.41µm and a nominal focal length of 9 mm). The first system (S1) integrates a RTK GNSS Emlid Reach RS2 receiver mounted on a geodetic pole whereas the second (S2) features a PPK GNSS hand-crafted device consisting of an Emlid Reach M2 module, the Emlid Reach M2 camera hotshoe adaptor, a cable for power bank supply, a camera flash adapter and a multi-band helical GNSS antenna). Images are acquired with the two proposed systems and the derived photogrammetric dense point clouds are assessed with respect to a GeoSlam Zeb Horizon point cloud.

System	*Camera*	*GNSS*
S1	Sony ZV1	Emlid Reach RS2 (RTK)
S2	Sony ZV1	Emlid Reach M2 (PPK) with a multi-band GNSS helical antenna

Table 1: Proposed GNSS-aided close-range photogrammetry systems for the 3D documentation of buildings.

Figure 1: The two systems in action (S1, left and S2, right).

2. THE PROPOSED GNSS-INTEGRATED PHOTOGRAMMETRIC SYSTEMS

The fundamental principle of a GNSS-assisted approach for close-range photogrammetry is to accurately determine the 3D coordinates of the digital camera's center of projection (COP), directly in the field by GNSS RTK/PPK technology. These positions are subsequently employed as constraints in the bundle block adjustment (BBA).

2.1 RTK system

The S1 system features the following components: a Sony ZV1 digital camera, a smallrig cage, an Emlid Reach RS2 GNSS receiver connected with the cage with a Reach RS2 thread adapter. The geodetic pole is connected to the cage with a screw thread adapter of 5/8″-1/4″ (Figure 2). The integrated system is very easy to transport, weighing around 1.9 kg including the GNSS receiver and the system autonomy is ca 22 hours.
Once mounted (Figure 1-left), the pole and the COP are on the same axis, but between the GNSS antenna phase center and the COP there is a small offset (Figure 2c). The vertical and horizontal offset between the antenna phase center and the COP was determined with millimeter precision using a caliper.

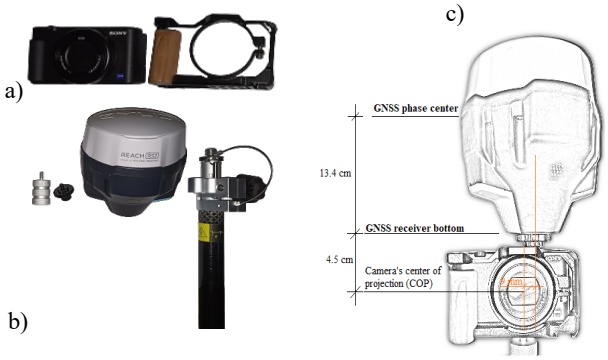

Figure 2: Components of the RTK system S1: the Sony ZV1 digital camera and the SmallRig cage (a), the screw thread adapter, the Reach RS2 thread adapter, the Emlid Reach RS2 GNSS receiver and a geodetic pole (b). The vertical and horizontal offset between the COP and the GNSS antenna phase center (c).

2.2 PPK system

The principle of the S2 system (Figure 3) is the same as for S1, but the lever-arm between the COP and the phase center of the GNSS antenna is calculated by calibration. Every time an image is taken with the Soy camera, a pulse is produced on the flash hot-shoe connector, which is synchronized with the shutter opening. The Reach M2 module records flash sync pulses with sub-microsecond precision, saving them in a raw data RINEX log stored in its internal memory.

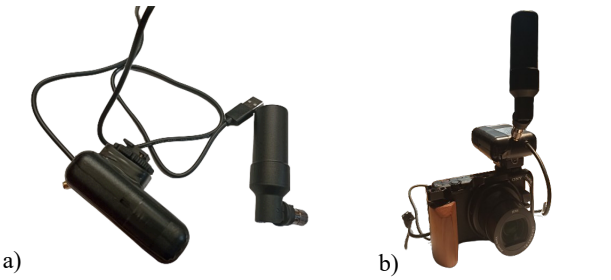

Figure 3: Components of the PPK system S2: (a) Emlid Reach M2 module, with the Emlid Reach M2 camera hot-shoe adaptor (inside the receiver) and a multi-band GNSS antenna (a). The integrated system with the Sony camera (b).

3. CASE STUDY AND DATA ACQUISITIONS

3.1 Study area

The building under study is the church of the Galata Monastery, built between 1582 and 1584, and listed in the National Register of Historic Monuments (Figure 4). The monastery is located on the top of Galata Hill in Iasi (Romania). Encircled by walls featuring loopholes and having a bell tower at the entrance, the Galata Monastery resembles a fortress. It has historically served as both a defensive structure and, at times, as a royal residence. Being a representative monument of Moldovan architecture from the late 16th century with the walls of the church adorned with two rows of arcades and covered with bas-reliefs rich in fine detail, the “Galata monastery” is considered a complex scene.
The monument was surveyed with the two proposed integrated systems (Section 3.2 and Section 3.3) as well as with a hand-held mobile laser scanner (Section 3.4) and UAS (Section 3.5).

Results and comparisons are reported in Section 4. The goal is to show the potential of the two integrated systems and their accuracy potential, hence the acquisitions performed with the two systems are slightly different as we are not aiming to compare the two systems among them.

Figure 4: The church of the Galata monastery.

3.2 Data acquisition with system S1

Using the S1 system (RTK GNSS-assisted), 41 images were acquired from different positions around the building with the pole levelled at a distance of approximately 20 m from the façade (resulting in the ca 5 mm GSD).
To assess the accuracy of the image block georeferencing process, 10 check points (ChPs) were distributed in the church proximity, materialized by plexiglass plates (Figure 6c) and measured with GNSS-RTK Emlid Reach RS2 receiver.
Each image acquisition position is measured by RTK GNSS using a three seconds average.

3.3 Data acquisition with system S2

A total of 68 images were acquired with the hand-held device, at approximately 15 m distance from the facades (ca 4 mm GSD).
During the image acquisition process, an Emlid Reach RS2 GNSS receiver was configured as the base station to record GNSS observations. The receiver's position was determined with GNSS-RTK technology at 2-minute intervals and a frequency of 5 Hz (601 measurements). Corrections were applied through the ROMPOS service, utilizing data from the permanent reference station, specifically the IASI station from the national geodetic network, situated 2.2 km away from the study area. To check the accuracy of the georeferencing process, ChPs are placed on the ground and measured with a GNSS-RTK Emlid Reach RS2 receiver.
The PPK GNSS measurement device has both horizontal and vertical offsets with respect to the COP, which will be determined with a calibration process. The lever-arm was also in first approximation measured with a caliper.

3.4 Data acquisition with the GeoSLAM Zeb Horizon

The GeoSLAM Zeb Horizon is a handheld LiDAR scanner designed for rapid 3D mapping and surveying. It features scanning capabilities within a 360° x 270° field of view, reaching a maximum range of 100 m and an ability to collect approximately 300,000 points per second. The declared relative accuracy ranges from 1 to 3 cm (GeoSLAM Ltd., Nottingham, UK) (Figure 5). The "Galata church" was scanned in approximately 10 minutes following two walking paths (Figure 5c). All scanning profiles are merged automatically by the instrument processing tool and ca 85 mil points are acquired. The laser scanning of the building encompassed the full reconstruction of the facades but was incomplete for the towers and the roof surface.

(a) (b) (c)

Figure 5: Data acquisition using the GeoSLAM Zeb-Horizon mobile scanner (a-b). Trajectory and point cloud displayed in real time on the system's mobile app (c).

3.5 Data acquisition with DJI Phantom 3 Standard

To obtain a complete reference point cloud of the church, an UAS flight was conducted with the DJI Phantom 3 Standard platform (Figure 6a). The drone features a built-in camera with a 3-axis stabilization gimbal (6.2 x 4.6 mm imaging sensor, 4000x3000 px images). The flight was conducted in manual mode at ca 20m above the ground and lasted approximately 16 minutes. A total of 31 images were acquired from different camera positions arranged in a circle around the building (Figure 6b). Before conducting the UAS flight, eight GCPs were measured around the church, using plexiglass plates featuring two black and orange triangles (Figure 6c). The GCPs positions were surveyed using a multi-band Emlid Reach RS2 GNSS receiver with centimetric accuracy, utilizing the Romanian Positioning Determination System (ROMPOS) with GNSS-RTK technology. Out of the 8 GCPs, four are employed as constraints in the Bundle Block Adjustment process, and the remaining four are used as Check Points (ChPs) for assessing the quality of the UAS image georeferencing process.

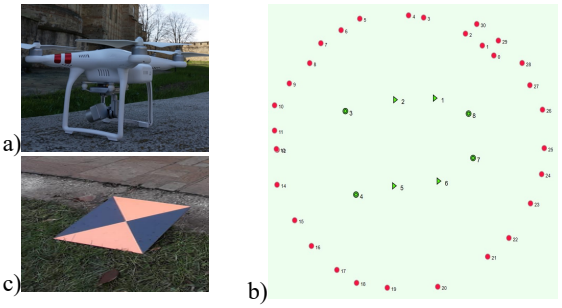

a) c) b)

Figure 6: The employed UAS platform (a), the camera network and ground points (b) and the plexiglass plate used for GCP measurements (c).

4. PROCESSING, RESULTS AND EVALUATION

4.1 3D surveying with the hand-held laser scanner

The registered point cloud (Figure 7a) is given in a local coordinate system, with origin at the start/end position of the walking path. To roto-translate it into the global reference system of the project, some GCPs are used within a Helmert transformation. The residuals of the transformation on ChP resulted in 4 mm, 2.2 cm and the 1.7 cm in the X, Y and Z direction, respectively. From the entire terrestrial scanning, ca 23 mil points are selected as belonging to the monument (Figure 7b).

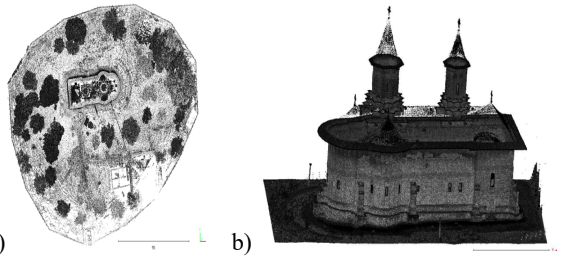

a) b)

Figure 7: The overall GeoSLAM point cloud seen from above (a) and a close-view of the church (b).

4.2 UAS image processing

The UAS image processing was carried out using Reality Capture software. A self-calibrating bundle adjustment with 4 GCPs and 4 ChPs was executed resulting in RMSEs of 1.9 cm, 1.0 cm and 3.3 cm in the X, Y and Z direction, respectively. The computed dense point cloud resulted in ca 800.000 points (Figure 8).

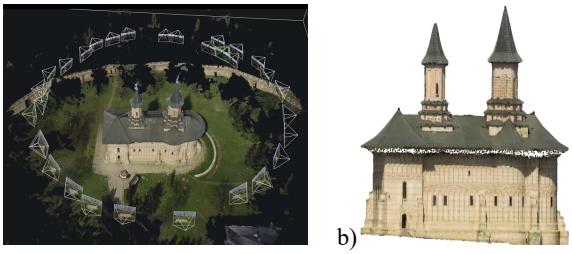

a) b)

Figure 8: Camera poses and dense point cloud of the UAS dataset.

4.3 Point clouds fusion for reference data

Considering that the UAS flight and the GeoSLAM acquisitions were performed in different days and their processing executed with different GCPs, a fine registration process for the two clouds was necessary. Indeed, a cloud-to-cloud comparison of the UAS and GeoSLAM point clouds (Figure 9) resulted in a standard deviation of 5.3 cm.

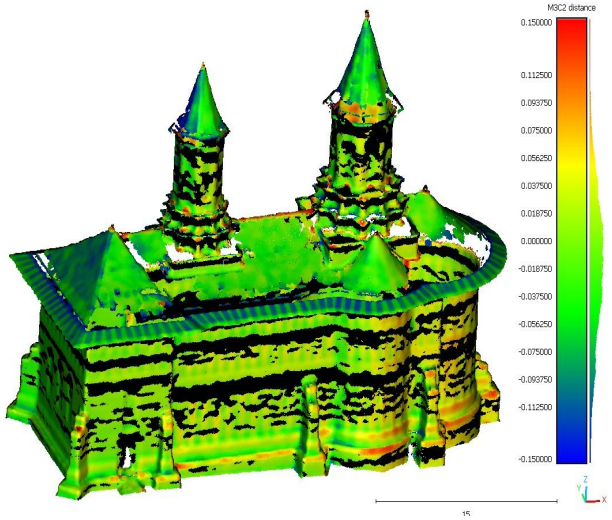

Figure 9: Color-coded M3C2 distances between the UAS and GeoSLAM point clouds.

Longitudinal and transversal cross-sections (Figure 10) also shown some discrepancies between the terrestrial and UAS point clouds.

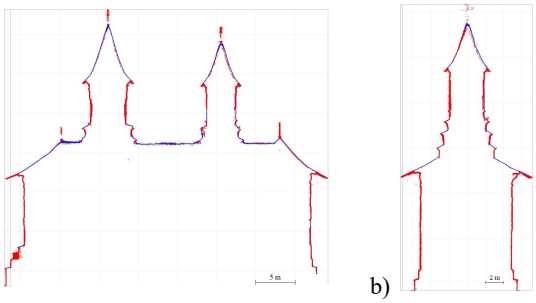

a) b)

Figure 10: Cross-sections for the GeoSLAM (red colour) and UAS (blue colour) point clouds before the precise alignment along longitudinal (a) transversal (b) direction of the church.

Therefore, to improve the alignment of the two point clouds, the Iterative Closest Point (ICP) algorithm available in OPALS (2024) is used. The standard deviation after five iterations is 2.5 cm (Figure 11).

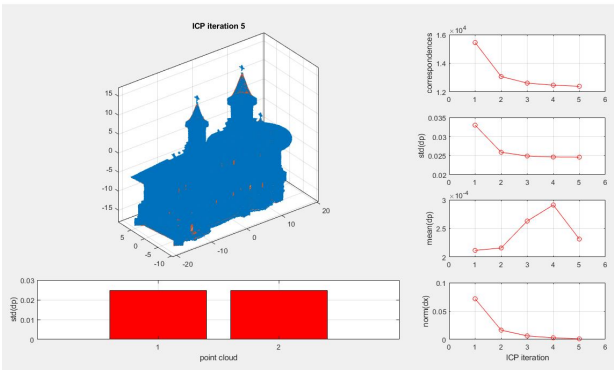

Figure 11: ICP results for the fused point clouds.

After the precise alignment, the two point clouds are again compared using the M3C2 distance. A threshold value of 2.5 cm is imposed and points exceeding this threshold are exported and integrated with the terrestrial GeoSLAM point cloud. The resulting fused point cloud is illustrated in Figure 12.

Figure 12: The fused point cloud of the church: UAS points (blue color) and GeoSLAM point cloud (brown color).

4.4 Processing of S1 data

The acquired images are processed in Agisoft Metashape, using the 3D coordinates of each COP as constraints in the BBA process (Figure 13). The vertical offset between the bottom of the GNSS antenna and the COP, as depicted in Figure 2c, is subtracted directly from the measured Z coordinates, considering

that the antenna height is set to 0 when recording the camera positions in the field. On the other hand, the horizontal offset of 9 mm is applied on the X axis using the *Camera Calibration* menu from Agisoft Metashape, before processing the images.

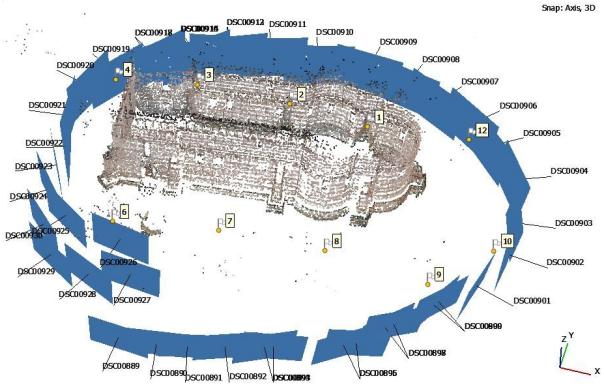

Figure 13: Camera poses and sparse point cloud for the S1 image dataset.

RMSEs, calculated by comparing the estimated position of the ChPs in the image block to the coordinates measured by GNSS RTK technology, yielded values of 1.6 cm, 2.4 cm and 1.7 cm in the X, Y and Z direction, respectively.
After a dense image matching, the photogrammetric reconstruction from the S1 data is compared to the fused point cloud (Section 4.3) using the M3C2 distances and a standard deviation of 1.8 cm is obtained (Figure 14).

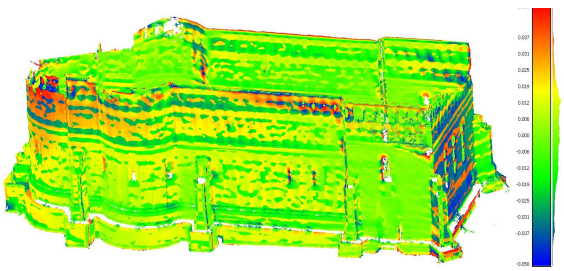

Figure 14: The dense point cloud obtained with S1 compared to the GeoSLAM point cloud (M3C2 distances).

4.5 Processing of S2 data

4.5.1 System calibration

The lever-arm calibration process is performed following the steps described in Morelli et al. (2022) for kinematic approach. A number of targets (GCPs) are placed on the ground and are surveyed with the Emlid Reach RS2 GNSS receiver for one minute, while almost 90 photos are acquired as shown in Figure 15 and 16. Each photo also has its corresponding GNSS PPK coordinates. The PPK GNSS device trajectory is computed using the kinematic processing option of Emlid Studio 1.7 software (Figure 17). The base station is the Emlid Reach RS2 GNSS receiver mounted close to the calibration field. So, using the observation and the navigation files downloaded from the Reach M2 module and the RINEX file downloaded from the Emlid Reach RS2 base station, the trajectory is processed, each camera position being stored as a separate event in the “*events.pos” file (Figure 15b). The solution was 93.8% fix, so only 6 camera positions from the total of 97 were float (orange color in Figure 15).
The calibration process was performed using the Metashape software, with the GCPs being manually measured in each image. The recovered camera positions and orientations after the BBA, together with the GCPs locations, are shown in Figure 16.

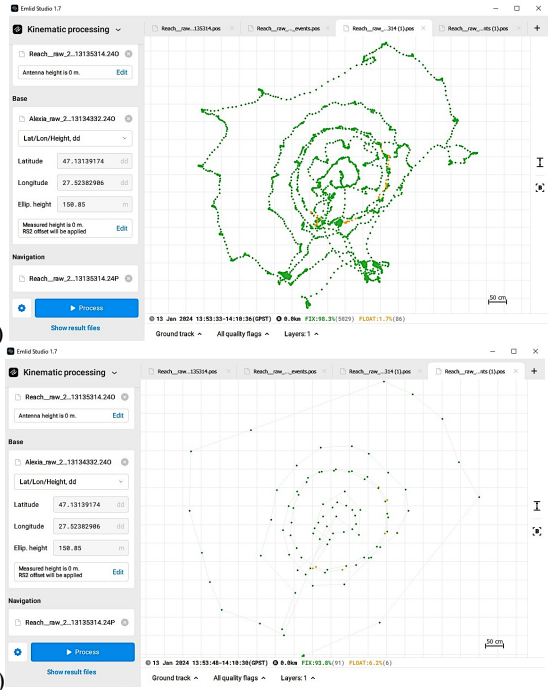

Figure 15: Kinematic processing of the PPK GNSS device trajectory with Emlid Studio 1.7 software: trajectory with calculated positions at every 0.05 s (a), the calculated positions for every image acquisition position (b).

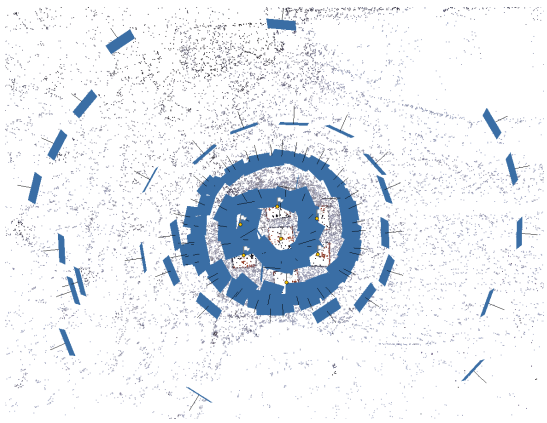

Figure 16: Camera network for the lever-arm estimation in the kinematic approach.

Using or not the GCPs in the lever-arm calibration process the lever-arm estimated is almost the same, probably because of the good camera network. The calculated lever-arm resulted as (X,Y,Z) = (-0.0197,0.1501,0.0073) meters.

4.5.2 Photogrammetric processing

The PPK GNSS device trajectory is computed as described in the system calibration phase (Section 4.5.1). The base station is the Emlid Reach RS2 GNSS antenna mounted in the church yard and the solution is 100% fix (Figure 17).
The 68 images acquired with the proposed PPK-GNSS device are processed in Agisoft Metashape without using GCPs. The 3D coordinates of each COP are used as constraints in the BBA process (Figure 18). Prior to image processing, the calculated lever-arm offsets between the COP and the antenna phase center are applied using the *Camera Calibration* menu in Agisoft Metashape.

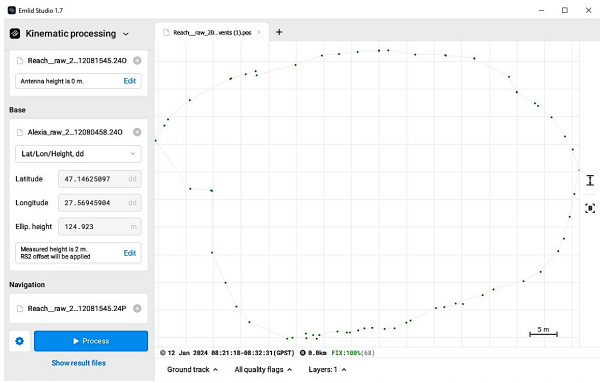

Figure 17: The calculated positions for every S2 image acquisition position by kinematic processing.

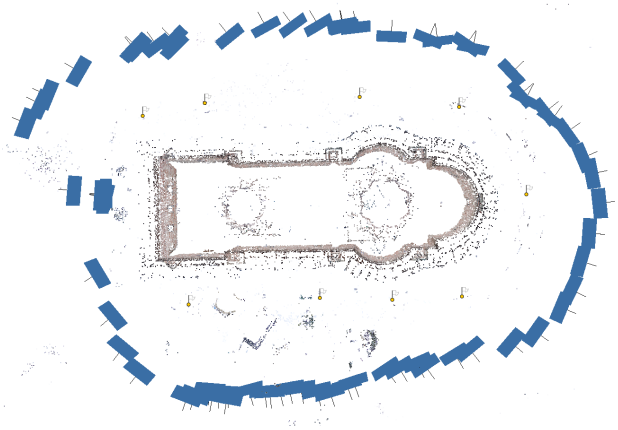

Figure 18: Camera poses and sparse reconstruction for the S2 dataset.

The residuals on camera locations are 0.8 cm on X axis, 0.7 cm on Y axis and 1.2 cm on Z axis. The RMSE values for the ChPs are 1.5 cm in X direction, 2.4 cm in the Y direction and 1.7 cm in the Z direction, with a total error of 3.3 cm. The results are in line with the results obtained with the RTK GNSS S1 system (Section 4.4).

However, the precision of RTK measurements may be influenced by various factors, including ionospheric errors, tropospheric errors, signal obstructions, and multipath errors (Baybura et al., 2019). These errors can arise due to features near the receiver, such as tree canopies and tall buildings, potentially impacting measurement quality. Therefore, it is important to note that the ChPs were strategically positioned in the vicinity of the church to ensure visibility in the images. Additionally, the churchyard features tall trees, which may impact the GNSS measurements and should be taken into consideration.

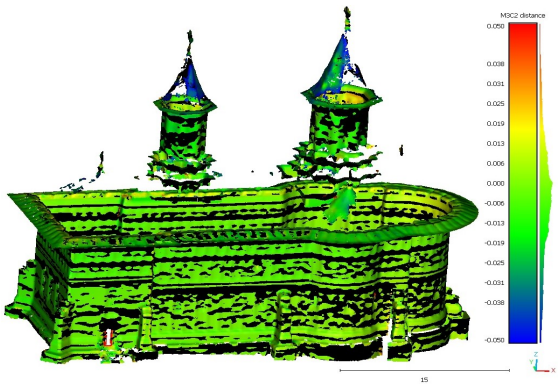

Figure 19: M3C2 distances between S2 and reference cloud.

Comparing the dense point cloud created with the S2 data with the reference point cloud (Section 4.3) using M3C2 distances, a standard deviation of 1.9 cm is obtained (Figure 19).

Without applying lever-arm calibration during the photogrammetric adjustment and solely considering the antenna height when calculating the positions of each image acquired with the PPK GNSS device through kinematic processing, the RMSEs on ChPs are 1.5 cm along the X, 2.2 cm along the Y and 3.1 cm along the Z, with a total error of 4 cm.

5. CONCLUSIONS

The process of 3D building modeling plays a pivotal role across a wide range of industries, contributing to improve documentation, conservation, design, visualization, and communication in various applications. It is of high importance to establish a comprehensive procedure that minimizes survey expenses and time requirements for 3D surveying processes. For these reasons, we have proposed two integrated measurement devices, relying on a digital camera and an RTK or PPK GNSS receiver to perform photogrammetric tasks without the use of GCPs for scaling and georeferencing purposes. The RMSEs evaluated on some 10 ChPs, proved the efficiency of the proposed devices (Table 2). In future studies, we plan to broaden the experiment to other more complex and large scenarios and to enhance the accuracy of the ChPs using a total station, in order to mitigate potential errors associated with RTK measurements.

System	# img	avg GSD	RMSEx	RMSEy	RMSEz
S1	69	5 mm	1.6 cm	2.4 cm	1.7 cm
S2	68	4 mm	1.5 cm	2.4 cm	1.7 cm

Table 2: Summary and comparison of achievements.

ACKNOWLEDGMENTS

The work was supported by a grant of the Ministry of Research, Innovation and Digitization, CNCS-UEFISCDI, project number PN-III-P1-1.1-TE-2021-1185, within PNCDI III.

REFERENCES

Baybura, T., Tiryakioğlu, İ., Uğur, M.A., Solak, H.İ., Şafak, Ş., 2019. Examining the accuracy of network RTK and long base RTK methods with repetitive measurements. *J. Sens.*, 3572605.

Brush, J.A., Pavlis, T.L., Hurtado, J.M., Mason, K.A., Knott, J.R., Williams, K.E., 2019. Evaluation of field methods for 3-D mapping and 3-D visualization of complex metamorphic structure using multiview stereo terrain models from ground-based photography. *Geosphere*, 15, 188–221.

Eker, R., 2023. Comparative use of PPK-integrated close-range terrestrial photogrammetry and a handheld mobile laser scanner in the measurement of forest road surface deformation. *Measurement*, *206*, p.112322.

Emlid—Available online: https://store.emlid.com/eu/product/reachm2-uav-mapping-kit/

Forlani, G., Pinto, L., Roncella, R. and Pagliari, D., 2014. Terrestrial photogrammetry without ground control points. *Earth Science Informatics*, *7*, pp.71-81.

Girardeau-Montaut, D., 2014. CloudCompare. http://www.danielgm.net/index.php

Jaud, M., Bertin, S., Beauverger, M., Augereau, E., Delacourt, C., 2020. RTK GNSS-Assisted Terrestrial SfM Photogrammetry without GCP: Application to Coastal Morphodynamics Monitoring. *Remote Sensing*, 12, 1889.

Morelli, L., Menna, F., Vitti, A. and Remondino, F., 2022. Action Cams and Low-Cost Multi-Frequency Antennas for GNSS Assisted Photogrammetric Applications Without Ground Control Points. *The International Archives of the Photogrammetry, Remote Sensing and Spatial Information Sciences*, *48*, pp.171-176.

Nesbit, P.R., Hubbard, S.M. and Hugenholtz, C.H., 2022. Direct georeferencing UAV-SfM in high-relief topography: Accuracy assessment and alternative ground control strategies along steep inaccessible rock slopes. *Remote Sensing*, 14(3), p.490.

Nocerino, E., Menna, F., Remondino, F., 2012. GNSS/INS aided precise re-photographing. *Proc. 18th IEEE Intern. Conference on Virtual Systems and MultiMedia (VSMM)*, pp. 235-242.

Oniga, V. E., Morelli, L., Macovei, M., Chirila, C., Breaban, A. I., Remondino, F., Sestraş, P., 2023. PPK processing to boost UAS accuracy in cadastral mapping, *The International Archives of Photogrammetry, Remote Sensing and Spatial Information Sciences,* XLVIII-1/W1-2023, pp. 345–352.

OPALS Orientation and Processing of Airborne Laser Scanning Data, 2024. Available online: http://geo.tuwien.ac.at/opals/html/ModuleGrid.html

Previtali, M., Barazzetti, L., Roncoroni, F., Cao, Y. and Scaioni, M., 2023. 360° Image Orientation and Reconstruction with Camera Positions Constrained by Gnss Measurements. *The International Archives of the Photogrammetry, Remote Sensing and Spatial Information Sciences*, *48*, pp.411-416.

Przybilla, H.J., Bäumker, M., Luhmann, T., Hastedt, H. and Eilers, M., 2020. Interaction between direct georeferencing, control point configuration and camera self-calibration for RTKbased UAV photogrammetry. *International Archives of the Photogrammetry, Remote Sensing and Spatial Information Sciences*, 43-B1-2020, 485-492.

Teppati Losè, L., Chiabrando, F. and Giulio Tonolo, F., 2020. Boosting the timeliness of UAV large scale mapping. Direct georeferencing approaches: Operational strategies and best practices. *ISPRS International Journal of Geo-Information*, 9(10), p.578.

Teppati Losè, L., Chiabrando, F. and Maschio, P., 2023. Direct georeferencing approaches for close-range and UAV photogrammetry in the built heritage domain. *The International Archives of the Photogrammetry, Remote Sensing and Spatial Information Sciences*, *48*, pp.1557-1564.

Xue, J., Hou, X., Zeng, Y., 2021. Review of Image-Based 3D Reconstruction of Building for Automated Construction Progress Monitoring. *Applied Sciences*, 11, 7840.

Ying, Y., Koeva, M., Kuffer, M., Zevenbergen, J., 2023. Toward 3D Property Valuation - A Review of Urban 3D Modelling Methods for Digital Twin Creation. *ISPRS International Journal of Geo-Information*, *12*, 2.

Wang, R., 2013. 3D building modeling using images and LiDAR: a review. *International Journal of Image and Data Fusio*n, 4:4, 273-292.

ZEB Horizon GeoSLAM, 2024. Available online: https://geoslam.com/solutions/zeb-horizon/

Zeybek, M., 2021. Accuracy assessment of direct georeferencing UAV images with onboard global navigation satellite system and comparison of CORS/RTK surveying methods. *Measurement Science and Technology*, 32(6), p.065402.

Zeybek, M., Taşkaya, S., Elkhrachy, I. and Tarolli, P., 2023. Improving the Spatial Accuracy of UAV Platforms Using Direct Georeferencing Methods: An Application for Steep Slopes. *Remote Sensing*, 15(10), p.2700.